1 Imaginary Wilson coefficients and R_K observables

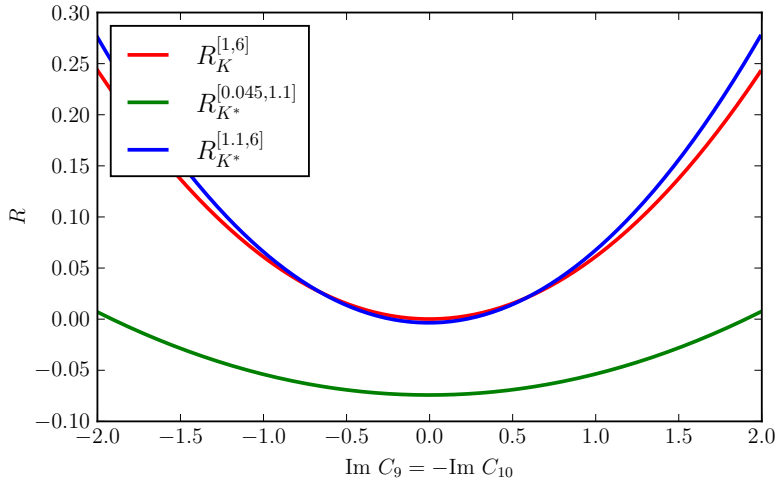

Figure 1: Values of R_K and R_{K^*} whith imaginary Wilson coefficients.

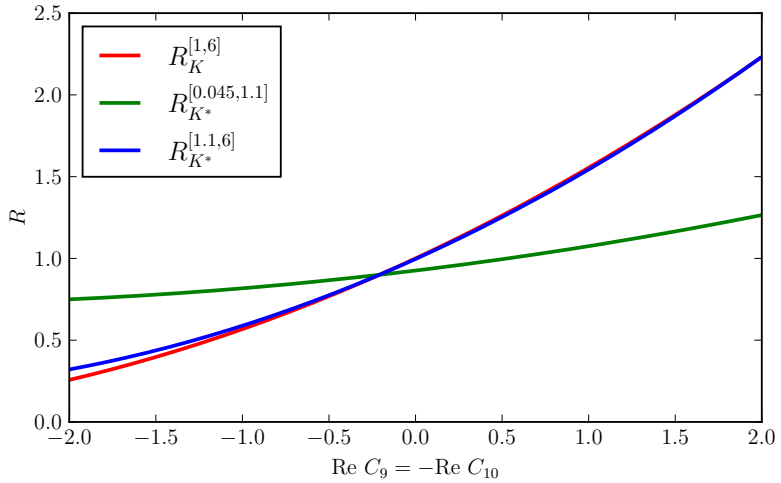

Figure 2: Values of R_K and R_{K^*} whith real Wilson coefficients.

Figure 1 shows the values of the ratios R_K and R_{K^*} in their respective q^2 ranges, when both Wilson coefficients C_9 and C_{10} are imaginary, and also we assume $C_9 = -C_{10}$. In all cases the minimum value for the ratio is attained at the SM point $C_9 = -C_{10} = 0$. The addition of non-zero imaginary Wilson coefficients results in larger values of R_K and R_{K^*}, at odds with the experimental values $R_{K^{(*)}}^{\text{exp}} < R_{K^{(*)}}^{\text{SM}}$. In contrast, when the Wilson coefficients are real as in Figure 2, values of $R_{K^{(*)}} \sim 0.7$, as in the experimental measurements, are possible.

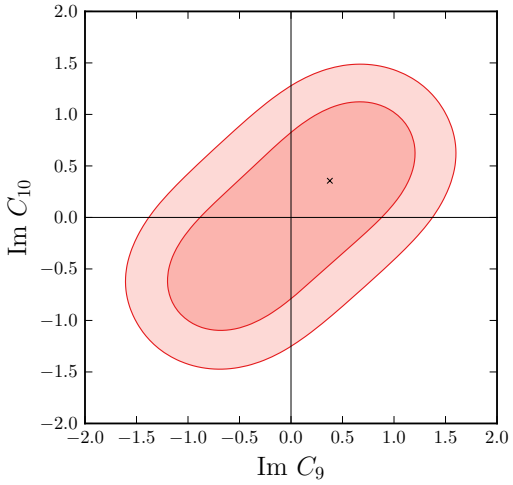

Figure 3: Allowed regions for imaginary Wilson coefficients.

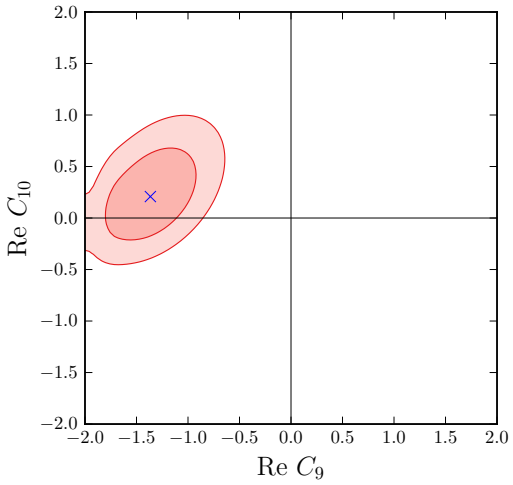

Figure 4: Allowed regions for real Wilson coefficients.

In Figure 3 we plot the allowed regions for imaginary values of C_9 and C_{10} when fitting to measurements of a series of $b \to s\mu^+\mu^-$ observables. In the fit we have included the ratios R_K and R_{K^*}, the angular observables P_4' and P_5'. The fit was carried by the software `flavio`, wich computes the χ^2 function with each (C_9, C_{10}) pair. The global minimum of the χ^2 was found at $C_9 = 0.41\,i$, $C_{10} = 0.42\,i$. The pull of the SM, defined as the probability that the SM scenario can describe the best fit assuming that $\Delta\chi^2 = \chi^2_{\text{SM}} - \chi^2_{\text{min}}$ follows a χ^2 distribution with 3 degrees of freedom, is of just $6 \times 10^{-4}\sigma$. That is, the SM result and the best fit are indistinguishable from an statistical point of view. The shaded regions in the plot are 1σ (darker pink) and 2σ (lighter pink) away from the best fit. Compare this to the fit to real values of the Wilson coefficients, in Figure 4. Now the confidence regions are much tighter and do not include the SM point. In fact, the best fit ($C_9 = -1.37$, $C_{10} = 0.21$) improves the SM by 3.49σ.

	Best fit	Pull ($\sqrt{\Delta\chi^2}$)
C_9^μ	$-1.452 - 0.015i$	4.15
C_{10}^μ	$3.890 + 3.000i$	4.23
$C_9^\mu = -C_{10}^\mu$	$-0.812 - 0.0255i$	3.84
$C_9'^\mu$	$-0.197 + 4.79 \times 10^{-4} i$	0.54
$C_{10}'^\mu$	$0.367 - 0.0136i$	1.27
C_9^e	$-2.095 + 4.659i$	3.11
C_{10}^e	$-1.262 + 0.496i$	3.05
$C_9^e = -C_{10}^e$	$-1.983 + 4.121$	3.04
$C_9'^e$	$-0.344 + 3.579i$	3.04
$C_{10}'^e$	$0.325 + 3.585i$	3.05

Table 1: Best fits for scenarios with NP in one individual complex Wilson coefficient.

2 Z' fit

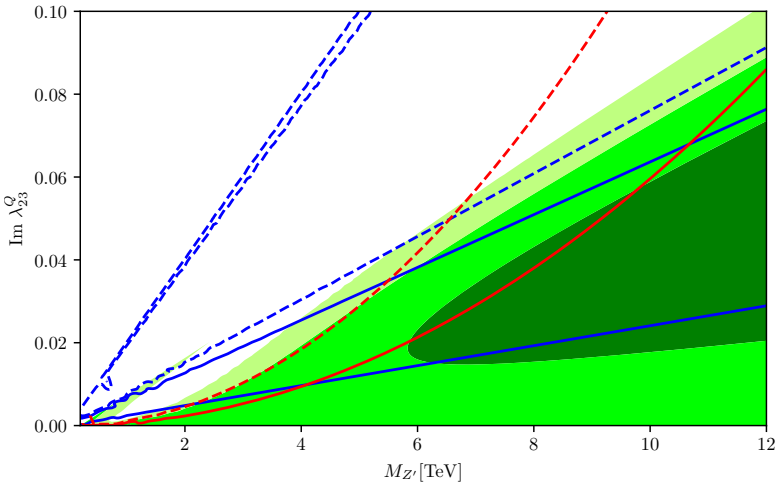

Figure 5: Bounds on Z' parameter space imposed by $b \to s\mu^+\mu^-$ decays and B_s mixing.

Figure 5 shows the bounds on the Z' mass $M_{Z'}$ and the imaginary coupling coupling λ_{23}^Q (setting $\lambda_{22}^L = 1$) imposed by $b \to s\mu^+\mu^-$ decays and B_s mixing. Blue lines correspond to the fit to B_s-mixing observables ΔM_s and $A_{\rm CP}^{\rm mix}$ (solid lines: $\Delta\chi^2 = 1$, dashed lines: $\Delta\chi^2 = 4$), red lines to $b \to s\mu^+\mu^-$ as in Figure 3 plus the branching ratios BR($B_s \to \mu^+\mu^-$) and BR($B^0 \to \mu^+\mu^-$) (solid lines: $\Delta\chi^2 = 1$, dashed lines: $\Delta\chi^2 = 4$), and green regions to the combined fit (dark green: $\Delta\chi^2 = 1$, medium green $\Delta\chi^2 = 4$, light green: $\Delta\chi^2 = 9$). The best fit for the $b \to s\mu\mu$ observables is the SM.

For the B_s-mixing observables, the best fit is found at $M_{Z'} = 10.6\,\text{TeV}$, $\lambda_{23}^Q = 0.051\,i$, which corresponds to $C_{bs}^{LL} = -1.63 \times 10^{-4}$. The SM has a pull of $\Delta\chi^2 = 1.78$. In addition to the best fit, there is a narrow fringe of allowed parameters when $C_{bs}^{LL} \sim -2.5 \times 10^{-3}$. In fact, both values of the Wilson coefficient can explain the measurement of $\Delta M_s^{\rm exp}$ using Equation 15 of 1712.06572.

The best fit when all observables are considered is found at $M_{Z'} = 12\,\text{TeV}$, $\lambda_{23}^Q = 0.054\,i$ (although the real best fit needs an even higher $M_{Z'}$), and the pull of the SM is $\Delta\chi^2 = 1.37$.

3 Leptoquark fit

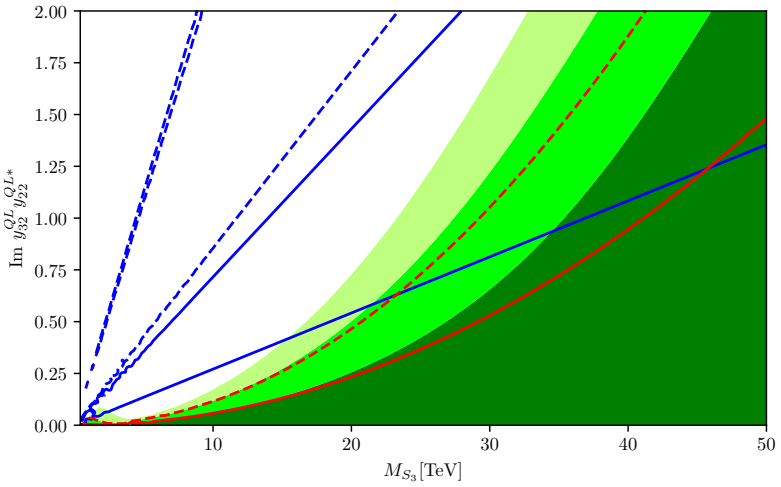

Figure 6: Bounds on S_3 leptoquark parameter space imposed by $b \to s\mu^+\mu^-$ decays and B_s mixing.

Figure 6 shows the bounds on the S_3 leptoquark mass M_{S_3} and the imaginary coupling coupling $y_{32}^{QL} y_{22}^{QL*}$ imposed by $b \to s\mu^+\mu^-$ decays and B_s mixing. The observables used in the respective fits are the same as in Figure 5. The SM scenario was prefered again by the $b \to s\mu\mu$ fit.

The fit to B_s-mixing observables is similar to the one in Z' models. The best fit is located $M_{S_3} = 19.6\,\text{TeV}$, $y_{32}^{QL} y_{22}^{QL*} = 1.06\,i$, with a SM pull of $\Delta\chi^2 = 1.78$.

The global fit leaves much more room for the SM scenario that the Z' model. The best fit is located at $M_{S_3} = 50\,\text{TeV}$, $y_{32}^{QL} y_{22}^{QL*} = 0.72\,i$, with a SM pull of only $\Delta\chi^2 = 2 \times 10^{-3}$.

Model	Mass	Best fit for coupling	$\Delta\chi^2$
Imaginary Z'	12 TeV	$0.054i$	1.37
Complex Z'	12 TeV	$0.007 + 0.051i$	3.32
Imaginary LQ	50 TeV	$0.72i$	2×10^{-3}
Complex LQ	9.79 TeV	$-0.13 - 0.09i$	23.07

Table 2: Best fits for some NP models.